Chitosan-hybrid poss nanocomposites for bone regeneration: The effect of poss nanocage on surface, morphology, structure and *in vitro* bioactivity

Sedef Tamburaci [a], Funda Tihminlioglu [b],*

[a] İzmir Institute of Technology, Graduate Program of Biotechnology and Bioengineering, Gülbahçe Campus, Urla, 35430 İzmir, Turkey
[b] İzmir Institute of Technology, Department of Chemical Engineering, Gülbahçe Campus, Urla, İzmir 35430, Turkey

ARTICLE INFO

ABSTRACT

POSS, regarded as the smallest silica particle, is widely used as nanofiller in polymer systems. POSS-based nanocomposites are deduced as novel materials having potency for biomedical applications owing to the enhanced biocompatibility and physicochemical characteristics. The aim of this work was to integrate the beneficial features of chitosan (CS) and OctaTMA-POSS nanoparticle to design nanocomposite for bone tissue regeneration. The nanocomposite scaffolds were fabricated by freeze-drying. The effects of POSS incorporation on morphology and structure of CS matrix were examined. Bioactivity and osteogenic effects of the POSS nanoparticles were investigated with cytocompatibility, cell proliferation, alkaline phosphatase activity, osteocalcin production and biomineralization assays. POSS incorporation altered the surface morphology by increasing surface roughness. Nanocomposite scaffolds with 82–90% porosity exhibited an increase in compression modulus of scaffolds (78–107 kPa) compared to control CS group (56 kPa). Results indicated that CS-POSS scaffolds were found cytocompatible with 3T3, MG-63 and Saos-2 cell lines. POSS incorporation showed promising effects on osteoblast adhesion and proliferation as well as increasing ALP activity, octeocalcin secretion and biomineralization of cells.

© 2019 Elsevier B.V. All rights reserved.

1. Introduction

Recently, natural polymer-based nanocomposites have come into prominence for bone tissue scaffold design. As a natural polymer, chitosan (CS) have promising characteristics such as non-toxicity, non-allergenicity, mucoadhesivity, biocompatibility and biodegradability. Moreover, CS mimics the main extracellular matrix components due to its similar structure with glycosaminoglycans. The ease of processing of CS into porous structure is another promising characteristic to fabricate a variety of scaffolds [1,2]. However, it has a limitation with mechanical properties compared to natural bone. Thus, CS is reinforced with an inorganic filler in order to overcome this limitation [1,3,4]. Nanofillers provide dramatic improvements in physical properties (thermal stability, mechanical properties, swelling behaviour) of polymer matrix and surface morphology by altering the structure at micro-nanoscale. Besides, recently bioactive nanofillers have come into prominence in scaffold designs for bone regeneration to provide mimicry with bone structure.

Among bioactive inorganic nanofillers, silica as the second most abundant biogenic mineral, show positive characteristics (biocompatibility, tunable surface area, ease of modification) for biomedical applications [5,6]. Silicon is widely distributed throughout the body especially in bone and connective tissue. It is extensively bound to gylycosaminoglycans, which are the main constituents in etxtracellular matrix (ECM) together with collagen and proteoglycans. Silicon supplementation is found as an effective treatment in osteoporosis that increases bone mineral density (BMD) and markers (pro-collagen type 1 N-terminal propeptide) that plays role in bone formation [7].

Literature studies found out the potential of silica based nanoparticles which show intrinsic bioactivity in hard tissue regeneration by conducing osteoblast differentiation and restraining osteoclast differentiation [8]. Silica nanoparticle incorporation in polymer matrix also supports bone cell adhesion and stimulates osteogenic responses and gene expression, especially inducing CaO deposition on material surface as well as providing enhancement in the structure by improving mechanical properties [9–11]. Recent studies confirmed the stimulating effect of orthosilicic acid on COL-1 secretion of human osteosarcoma and primary osteoblast like cells which induces osteoblastic differentiation [12]. In addition to this result, Dong and co-workers investigated the effect of

---

* Corresponding author.
E-mail address: fundatihminlioglu@iyte.edu.tr (F. Tihminlioglu).

silicon on BMP-2/Smad1/5/RUNX2 signaling pathway in COL-1 secretion of MG-63 and U2-OS cells and found that silicon increased the ALP activity and biomineralization by inducing COL-1 synthesis and osteocalcin secretion via BMP-2/Smad1/5/RUNX2 signaling pathway. It is also known that silicon can enhance calcium deposition at physiological doses. Literature studies also concluded that silicon bonds to calcium ions at the early stage of bone calcification [13]. Besides, silica nanoparticle incorporation alters the surface topography which is an crucial factor for cell attachment and spreading on biomaterial surface [14].

Particle size and morphology are significant characteristics that effect the bioactivity of silica particles in osteoblast differentiation [15]. The size of the nanoparticle also effects the surface roughness that has major role on osteoblast-material interaction in bone regeneration. However, nanoparticles weakly dispersed and tend to agglomerate in matrix due to their incompatibility with polymer structure. Thus, nanofillers are generally grafted or modified with organic groups compatible with the polymer matrix to overcome this problem [16]. Among modified silicate nanoparticles, organosilicates (R_n Si_n $O_{1.5n}$) with R groups are defined as silsesquioxanes. Polyhedral oligomeric silsesquioxane (POSS) regarded as the smallest possible silica particle (1.5 nm), is highly symmetrical molecule which possess hybrid (inorganic/organic) well-defined cage structure composed of silicon/oxygen cage and hydrocarbon functional groups attached to corner Si molecules. It has intermediate ($RSiO_{1.5}$) chemical composition, between silica (SiO_2) and silicone (R_2SiO) [17]. Thus, POSS nanoparticles could be interfused in polymer effectively via copolymerization, grafting or blending and shows performance region between polymers and ceramics [18–22]. The structure and bulk properties of POSS/polymer nanocomposites can be tailored by varying the R groups. The changes obtained in material characteristics predominantly hinge on the interactions between R groups and the polymer matrix serving as a reinforcing agent or a plasticizer [19,23–25]. POSS also influences the surface chemistry (wettability) and alters the surface roughness and topography of polymer matrix. These unique properties make POSS a potential nanomaterial for stimulation of biological responses at nanoscale. This stimulation leads to improvement in cell attachment and response for apatite formation [11,19].

Polymer/POSS nanocomposites can be utilized as, biomedical devices and biomaterials having tunable degradation rates required for tissue engineering applications [4,11]. So far, limited literature studies have been found with respect to polymer-POSS nanocomposites for bone and cartilage regeneration [4,24–27].

In our previous study, CS-POSS nanocomposite membranes as 2D structure showed promising effects on osteoblast-like cell attachment and proliferation for guided bone regeneration [28]. Hence, in this study, it is aimed to design a novel porous 3D CS-POSS nanocomposite scaffold to mimic the bone tissue which can induce biomineralization with unique silica hybrid structures as well as enhancing cell-material interaction at nanoscale. *In vitro* bioactivity of nanocomposite scaffolds was investigated extensively with MG-63 and Saos-2 as model cell lines showing different osteoblastic responses as well as human osteoblast cells (hFob). The effect of POSS incorporation on mechanical, physical and morphological properties of CS was evaluated. In addition, *in vitro* studies were performed to determine the cytotoxicity, bioactivity and osteogenic effects of POSS nanoparticles on bone tissue regeneration.

2. Material & method

Low molecular weight chitosan (50,000–190,000 Da; Sigma-Aldrich) and POSS Octa TMA® (Hybrid Plastics) were used for fabrication of nanocomposite scaffolds. Pierce BCA protein assay (Thermofisher Scientific) and Bovine Serum Albumin (BSA; Sigma-Aldrich) were used to detect protein adsorption. WST-1 (BioVision Inc.) and Resazurin (Cell Signaling Technology Inc.) cell viability kits, StemTAG™ Alkaline Phosphatase Activity (ALP) Kit (Cell Biolabs Inc.) and Human OC/BGP (Osteocalcin) ELISA Kit (Elabscience) were used for *in vitro* studies.

2.1. Scaffold fabrication

CS-POSS scaffolds were fabricated via freeze drying technique. POSS nanoparticles were incubated at 80 °C for 24 h to prevent moisture and agglomeration. CS was dissolved in 1% v/v acetic acid solution. POSS nanoparticles were dispersed in water. Then, CS solution and POSS dispersion were mixed. Ultrasonication method (Misonix Ultrasonic Liquid Processor, 30 min at 15 °C, 35 Amplitude) was used to distribute POSS nanoparticles in polymer matrix homogenously. Solution was moulded in well-plates and pre-freezed at −20 °C for 24 h. Then CS-POSS solution was freeze-dried for 48 h (Labconco Freezone, −46 °C, 0.01 mBar) and kept in dessicator. Fabricated scaffolds were neutralized with 1 M NaOH solution and washed with distilled water to remove residual NaOH.

2.2. Scaffold characterization

2.2.1. Particle size distribution, morphology and surface roughness

Morphology of POSS nanoparticles were dispersed with 0.001 and 0.0001% dilutions on TED Pella (UC-A on holey 400 mesh Cu) grids and observed with STEM. Average particle size of dispersed POSS nanoparticles was measured with Image J software. DLS analysis was performed (Malvern Zeta-sizer Nano ZS) to determine the hydrodynamic sizes of POSS nanoparticles. 1% w/v POSS dispersions were prepared with deionized water and incubated in ultrasonic bath for 5 min before testing. POSS nanoparticle morphology was observed with AFM analysis with tapping mode. In addition, CS-POSS membranes which were prepared by solvent casting technique were analysed to investigate the alterations on surface topography and roughness of CS matrix with POSS incorporation. The AFM topographic data and surface roughness (Rq) were analyzed quantitatively from three different areas with 5×5 μm dimensions. Nanoscope software (Digital Instruments Inc., USA) was used for calculations.

2.2.2. Scanning electron microscopy (SEM)

Scaffold morphology, pore wall surface structure and average lateral pore size were observed with SEM (Quanta FEG 250) analysis. Scaffolds were sputter-coated with thin gold layer (Emitech K550X) before analysis. Lateral pore size calculation was carried out with Image J software.

2.2.3. Fourier transform infrared spectroscopy (FTIR)

The chemical structure, characteristic peaks of POSS nanocages and alterations on chemical bonds of chitosan matrix after POSS incorporation were investigated with fourier transform infrared spectroscopy with ATR instrument (FTIR-ATR, Perkin Elmer) at wavenumber range of 4000–450 cm^{-1} with resolution of 16 cm^{-1} and scan number of 20.

2.2.4. Determination of scaffold porosity

Total porosity % and macro-micro pore range of scaffolds were evaluated via mercury intrusion porosimeter (Micromeritics, AutoPore IV). Scaffolds were analysed with low pressure to prevent the disruption of structure. MicroCT (Scanco-μCT 50) analysis was used to observe the 3D architecture and evaluate total porosity. Analysis was performed with native resolution at 45 kVp-88uA. Scaffolds were scanned through 500 slices using 3 μm voxel size.

Liquid displacement technique was used to evaluate open porosity. Sample was immersed in ethanol (V_1) and placed in vacuum oven to allow ethanol to penetrate the pores. Measured volume was recorded as V_2. Then scaffold was taken off. After scaffold removal, volume of remaining ethanol was measured (V_3). Open porosity of sample was calculated using the Eq. (1).

$$\varepsilon = (V_1 - V_3)/(V_2 - V_3) \tag{1}$$

2.2.5. Mechanical test

Compression test was performed in dry and wet conditions (TA XT Plus Texture Analyzer, ASTM-D 5024-95a standard) to investigate the mechanical properties of CS-POSS scaffolds. In wet condition, scaffolds were incubated PBS solution for 1 h prior to testing. Scaffolds were compressed up to 75% of original height with 5 mm/min cross-head speed.

2.2.6. Protein adsorption assay

Bovine serum albumin (BSA) solution was used for protein adsorption assay as standard. Samples were incubated in 0.1% BSA solution at 37 °C for 24 h. Protein assay was perfomed with BCA kit according to microplate procedure.

2.2.7. Enzymatic degradation

CS-POSS scaffolds were incubated in $1\times$ PBS solution (pH 7.4) at 37 °C with 1.5 μg/mL lysozyme to mimic the concentration in serum [29]. Sodium azide (0.01%) was added to enzymatic degradation solution to inhibit possible contamination. Enzymatic solution was changed three times a week to prevent the loss of enzymatic activity. Samples were taken off from solution at 7, 14, 21 and 28 days of incubation and dried. Weight loss % was evaluated using Eq. (2) as shown below; where W_o and W_1 are dry and wet weight of the samples, respectively.

$$Weight\ Loss\ \% = W_0 - W_1/W_0 \tag{2}$$

2.2.8. Swelling study

The effect of POSS nanoparticles on water uptake capacity of CS scaffolds was evaluated via swelling study. Scaffolds were incubated in $1\times$ PBS solution at 37 °C for 24 h. Dry weights of scaffolds were measured before incubation (Wd). Wet samples were weighed (Ww) after incubation. Swelling % was evaluated using Eq. (3):

$$Swelling\ \% = (Ww - Wd)/Wd \times 100 \tag{3}$$

2.2.9. Mineralization study

Exogenous mineralization on scaffolds was determined by incubating in m-SBF solutions ($1\times$ and $10\times$ m-SBF) at 37 °C to simulate the *in vivo* condition [30,31]. Mineralization study was evaluated for 14–21 days. SBF medium was changed every 48 h to provide the circulation and prevent the decrease of free calcium and phosphate ions during mineralization process. Mineral formation and calcium phosphate ratio on scaffold surface were observed via SEM, EDX and XRD analyses.

2.3. In vitro studies

MG-63, Saos-2 and hFob cell lines were used for *in vitro* studies MG-63 cell line was cultivated with MEM Eagle's whereas, DMEM was used for Saos-2 and hFob cells.

2.3.1. Cell attachment and spreading

MG-63 cells were seeded on scaffolds and incubated for 7 days to observe cell attachment and spreading. Cell fixation, fluores-cence staining and sample dehydration protocols were performed as mentioned in our previous study [32].

2.3.2. Cytotoxicity determination

WST-1 cell viability kit was used to investigate the cytotoxicity of scaffolds. Scaffolds were extracted in cell culture medium for 24 h with respect to ISO-10993 protocol. Extraction medium was used to culture cells for 72 h. Cell viability % was calculated using Eq. (4).

$$Cell\ viability\% = \frac{Average\ absorbance\ value\ of\ treated\ samples}{Average\ absorbance\ value\ of\ control} \times 100 \tag{4}$$

2.3.3. In vitro cell proliferation on composite scaffolds

Sterilization was carried out with incubation of scaffolds in 70% (v/v) ethanol overnight. Cell seeding on scaffolds was mentioned in our previous study in detail [32]. Fluorometric resazurin assay was carried out to detect cell proliferation with quantification of resorufin formation as relative fluorescence units (RFU).

2.3.4. Alkaline phosphatase (ALP) activity and osteocalcin secretion

hFob, MG-63 and Saos-2 cells were cultivated with osteogenic medium for 28 days. Intracellular ALP activity was evaluated with StemTAG™ ALP assay. Osteocalcin (OC) secretion was evaluated with Human OC/BGP ELISA assay by extracting cultivation medium from scaffolds.

2.3.5. In vitro biomineralization

Calcium and phosphate depositions were observed with Von Kossa (vK) and Alizarin Red S (ARS) staining methods [33]. Before staining, cell fixation was performed as mentioned in section 2.3.1. Scaffolds were stained with vK by incubation in 1% (w/v) aqueous silver nitrate (Sigma-Aldrich) for 30 min under UV light. Then samples were washed with distilled water and immersed in 5% (w/v) sodium thiosulfate (Sigma-Aldrich) for 5 min to eliminate unreacted silver. Calcium deposition on scaffolds was investigated with 2% (w/v) aqueous ARS (pH 4.1) staining. Scaffolds were incubated in the dark for 30 min and rinsed with distilled water several times. Calcium and phosphate depositions were viewed through stereomicroscope (Olympus SOIF DA 0737). ARS extracts were also analysed spectrophotometrically (405 nm) to specify the calcium mineral deposition difference semi-quantitatively.

2.4. Statistical analysis

All experimental groups were evaluated with three replicates. The experimental data was given with the standard error of mean (SEM). Results were analysed with one-way and two-way analysis of variance (ANOVA) using Tukey's multiple comparison test ($p < 0.05$).

3. Results and discussion

3.1. Characterization

3.1.1. Particle size distribution, morphology

Particle size is one of the important characteristics of silica nanoparticles that takes part in their intrinsic bioactivity in bone regeneration. Thus, morphology and size of POSS nanoparticles were investigated with STEM and DLS analyses. POSS nanoparticles possessed hydrodynamic size range of 1–250 nm by means of intensity. Non-aggregated POSS nanoparticles (15%) were observed with an average size of 1 nm similar to the literature [18]. In addi-

tion, 70% of POSS particles were found as aggregated forms (250 nm) due to the strong interaction between their reactive groups. The tendency of POSS nanoparticles to agglomeration is also observed as small aggregations (%15) with an average size of 12 nm similar to literature [34]. STEM images indicated that POSS agglomerations were observed with an average size of 65 ± 11.4 nm at 1:1000 dilution and POSS nanoparticles were dispersed at 1:10,000 dilution with an average size of 45 ± 7.4 nm (Fig. 1). The effect of silica nanoparticle size on osteoblast differentiation was investigated by Ha and co-workers. Results revealed that the change in silica nanoparticle size showed significant effects on osteoblast activity. They obtained highest inducing effect on osteoblast activity with 50 nm silica nanoparticles [15]. Thus, POSS nanoparticles incorporated in CS matrix were observed in effective size range.

3.1.2. Surface morphology and roughness

POSS nanoparticle morphology was also investigated with AFM analysis. POSS nanoparticles were dispersed in ultrapure water with 10^{-6} dilution ratio and dropped on coverslip. AFM images showed that POSS nanoparticles possessed spherical morphology with 30 ± 6.9 nm average particle size. Alterations on surface morphology of CS matrix with POSS incorporation was observed with CS-POSS membranes. POSS nanoparticles were distributed in polymer matrix by ultrasonic homogenization. AFM images showed that POSS nanoparticles altered the surface morphology by increasing roughness (Fig. 1). Mean roughness for CS membranes was found as 3.58 ± 0.1 nm. POSS nanoparticles were homogenously distributed on CS matrix for 10% (w/w) concentration. However, at 20% (w/w) concentration, POSS nanoparticles tend to interact with their organic R groups and started to agglomerate
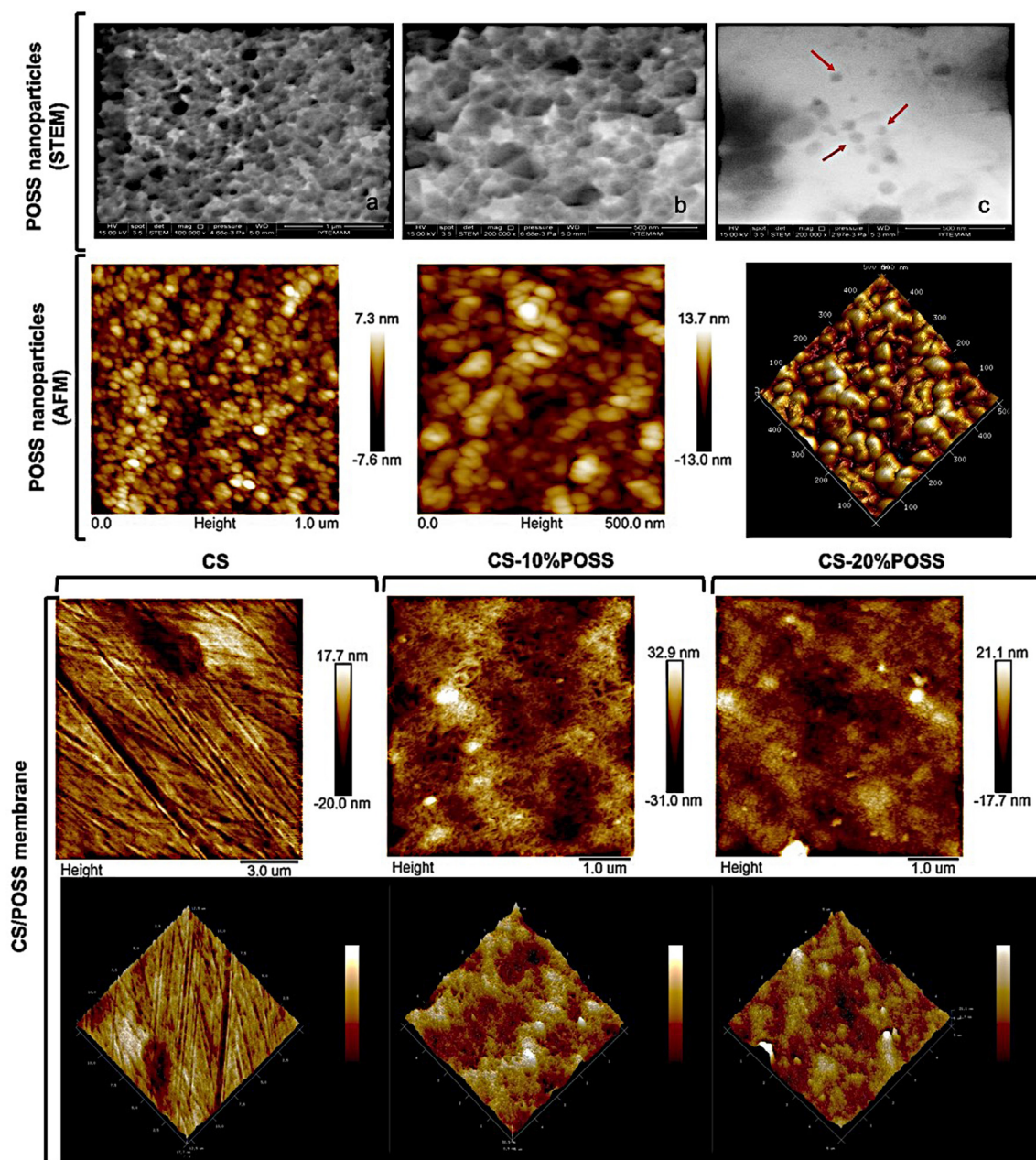

Fig. 1. STEM images of POSS nanoparticles with 1/1000 (a and b) and 1/10,000 (c) dispersions; AFM images of POSS nanoparticles and CS-POSS membranes, respectively.
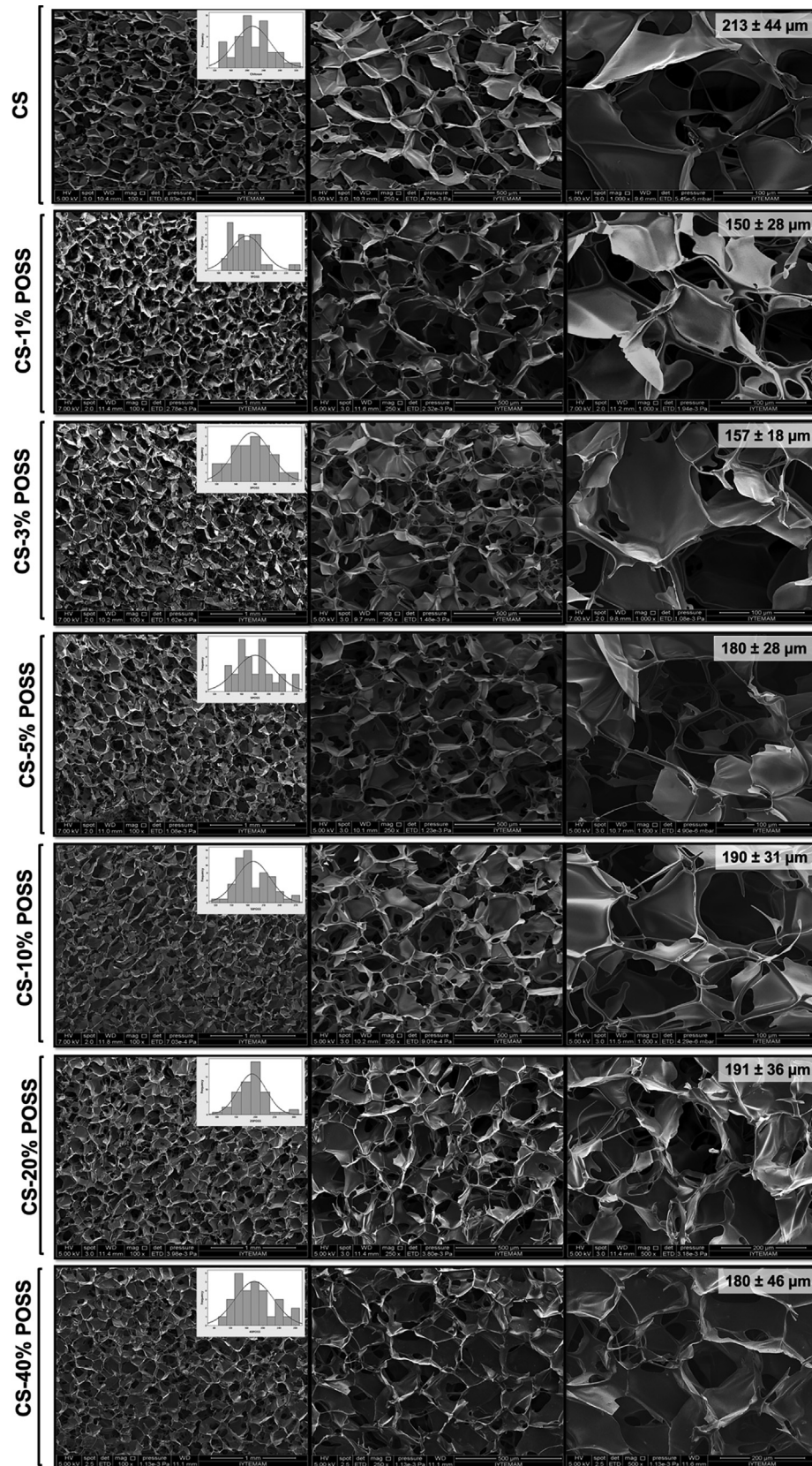
Fig. 2. Scanning electron micrographs of scaffolds with 100×, 250× and 1000× magnifications: CS; CS-1%POSS; CS-3%POSS; CS-5%POSS; CS-10%POSS; CS-20%POSS; CS-40% POSS respectively. Lateral pore size distribution and average pore size of groups were depicted on SEM images.
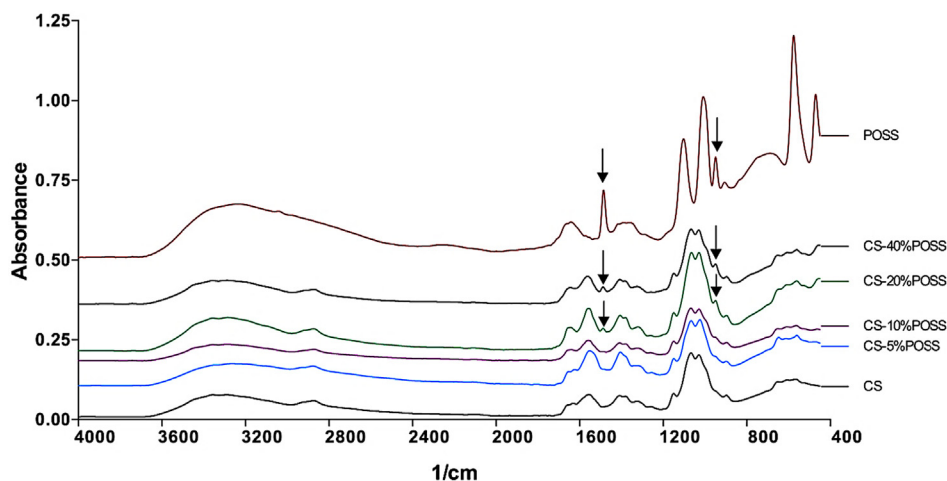
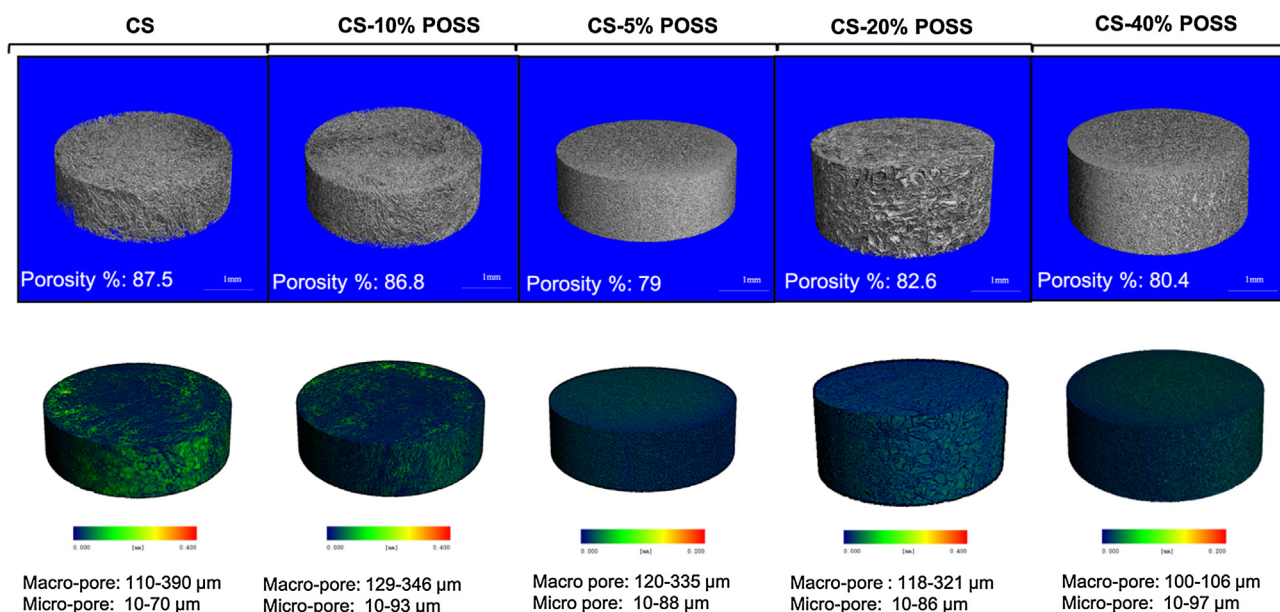**Fig. 3.** FTIR spectra of CS, POSS and CS-POSS nanocomposite scaffolds.

Fig. 4. Micro CT images of CS, CS-5%POSS, CS-10%POSS, CS-20%POSS and CS-40%POSS scaffolds (3D structure and colored pore size distribution). Total porosity, micro, and macro pore range of scaffolds were given respectively. (For interpretation of the references to color in this figure legend, the reader is referred to the web version of this article.)

in polymer matrix. These agglomerations caused non-homogenous distributions on surface and they were observed as embedded structures in polymer matrix. Thus, mean roughness of surface decreased slightly from 8.4 nm ± 0.01 to 6.3 ± 1.74 nm.

3.1.3. Scaffold morphology

SEM images showed that highly porous uniform CS-POSS scaffolds were fabricated via lyophilization technique. CS scaffolds possessed uniform porous structure with interconnections and average pore size was obtained as 213 ± 44 μm (Fig. 2a). POSS incorporation did not alter the microstructure and overall porosity of CS scaffold (Fig. 2). Average pore size of CS-POSS scaffolds were obtained in a range of 150–190 μm. However, at high POSS concentrations (20–40%) morphology changed and pore wall surfaces enlarged (Fig. 2 (f, g)). Similarly, the silica phase (TEOS, GPTMS) is indicated as a continuous phase which cover the chitosan pore walls without affecting the porosity significantly [35].

3.1.4. FTIR analysis

FTIR spectra of POSS, CS and CS-POSS nanocomposite scaffolds were shown in Fig. 3. Tetramethyl ammonium (NMe_4) functionalized POSS has a nanocage structure which is composed of rigid tetragonal Si—O cage having —$ON(CH_3)_4$ groups in each corner. The spectra results show the characteristic peaks of POSS nanocages at 470–570 cm^{-1} as Si—O—Si asymmetric stretching and bending vibrations. Peak at 1096 cm^{-1} is attributed to strong and symmetric Si—O—Si stretching absorption band of silsesquioxane cage. Torsional vibration of NMe_4 groups was observed at 945 cm^{-1}. Absorbing peaks at 1480 cm^{-1} are also attributed to the stretching vibration of organic NMe_4 group. Characteristic peaks of NMe_4 group were also observed at CS-POSS nanocomposites with high POSS contents. Basic characteristic peaks of chitosan were shown as C—H stretching at 2840 vibrations and stretching vibrations of OH groups at 3330 cm^{-1}. In addition, the bands at 1620 cm^{-1}, 1530 cm^{-1} and 1340 cm^{-1}were attributed to Amide I, —NH_2 bending and Amide III, respectively. FTIR spectra of CS-
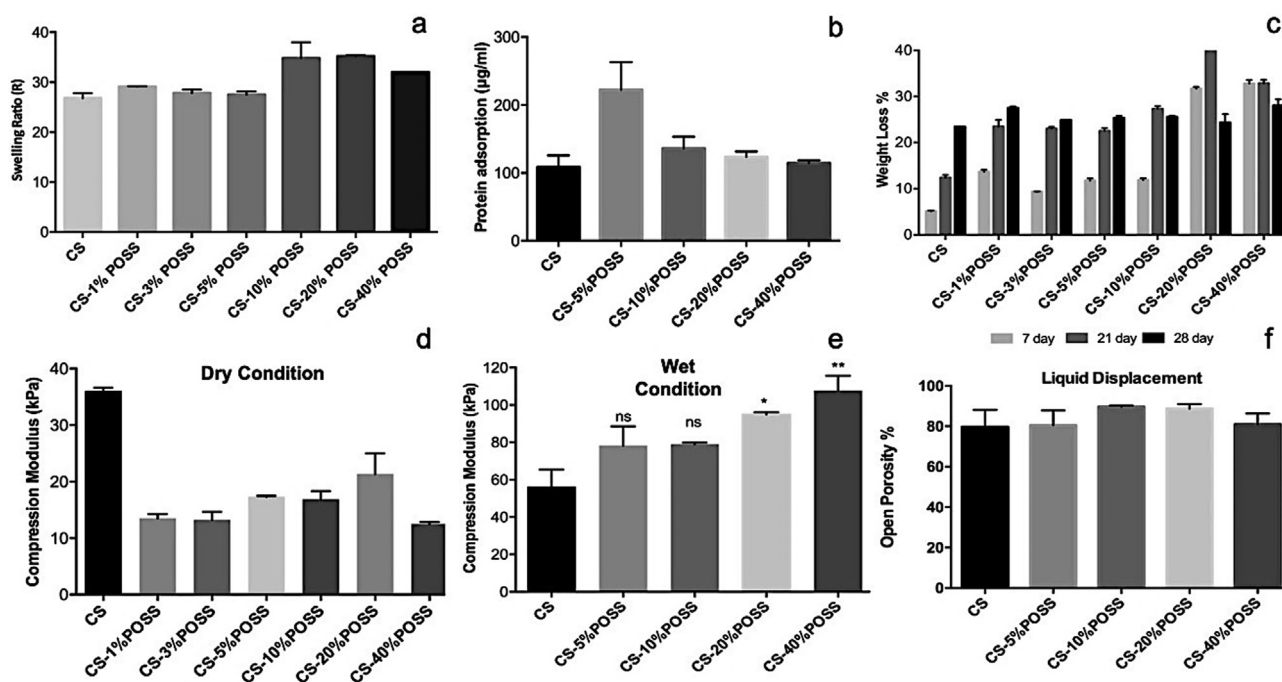
Fig. 5. Swelling ratio (a) and protein adsorption of scaffolds for 24 h (b); Scaffold weight loss % for 28 days (c), Compression moduli of scaffolds in dry (d) and wet (e) conditions; Open porosity of scaffolds (f) were depicted respectively.

POSS groups showed that POSS nanocages did not chemically interact with chitosan matrix.

3.1.5. Total and open porosity determination

An ideal bone scaffold must have interconntected micro and macro porous structure to provide optimum microenvironment for cell bioactivity and tissue regeneration. Microporosity (<100 μm) takes part in biomimetic structure of the biomaterial as well as the surface roughness and micropores can enhance cell-material interaction on surface. The macroporosity (100–500 μm) is required for vascularization and bone in-growth [36]. Open porosity, macro and micro pore ranges of scaffolds were determined with mercury porosimeter and data were given in supplementary file (Supplementary Table S1). However, mercury intrusion in polymeric scaffolds may lead to disruption of pore walls with applied pressure. Thus, liquid displacement method was used to verify the open porosity % of scaffolds. Results showed that CS-POSS scaffolds exhibited high porosity % with similar trend in different methods (Table S1). CS-POSS nanocomposites exhibited open porosity range as 79–90% and POSS nanocage addition to chitosan matrix slightly increased the porosity % of the structure (Fig. 5f).

CS-POSS scaffolds were also observed with micro-CT. CS-POSS scaffolds showed a morphology having micro-macro pores with high porosity range (83–88%) (Fig. 4). Increasing POSS concentrations decreased macropore size in the structure. Scaffolds showed a morphology with high porosity and interconnected pores whereas, increasing POSS content from 5 to 20 wt% changed the 3D structure with lower porosity (82.6%) and increased the pore size (Fig. 4). Pore wall surfaces increased and interconnections between pores decreased with increasing POSS content. This change in pore surface may arise from possible agglomerations of POSS nanoparticles on surface as indicated in AFM results. Similarly, 3D structure of silica-chitosan scaffolds was investigated by micro CT. High amount of silica caused a condensed silica network formation which interrupted ice crystallization and reduced the

pathway of growing ice crystals [37]. Similarly, Lu and co-workers fabricated hydroxypropyl chitosan/nanohydroxyapatite(n-HA) composite scaffolds and investigated the effect of n-HA content on porosity of scaffolds with micro-CT analysis. Results indicated that scaffold porosity decreased with increasing n-HA in polymer matrix [38]. 3D images indicated that scaffolds were fabricated as highly interconnected porous structures. Consequently, CS-POSS scaffolds were found to have appropriate porous structure to mimic trabecular bone having a porosity range of 50–90% and can allow cell migration, nutrient supply for bone cell growth [39].

3.1.6. Mechanical characterization

Compression moduli and strength of CS-POSS nanocomposites were evaluated in dry and wet state (Fig. 5). Dry CS-POSS scaffolds showed low modulus and mechanical strength compared to CS group. Besides, increasing POSS content induced a positive effect on mechanical characteristics up to 20%. Above this concentration, compression modulus decreased. In higher concentrations, tendency of POSS nanoparticles to bond with eachother through their R groups and to agglomerate in polymer matrix may affect the homogenity of nanocomposite structure. CS-POSS scaffolds possessed compression moduli and strength in a range of 13.5–20 kPa and 74–114.4 kPa, respectively. Statistically significant difference was obtained between CS and CS-POSS scaffolds (p < 0.0001). In contrary to dry condition, wet CS-POSS scaffolds showed higher compression moduli. POSS incorporation caused an elastic behaviour during compression and regaining the initial shape after compression. Increasing POSS content from 5 to 40% caused an increase in compression modulus of CS changing from 56.3 to 107.6 kPa with maximum POSS concentration. Wet CS-POSS groups (20% and 40%) possessed significantly higher moduli compared to CS (p < 0.05). In literature, the mechanical strength properties of CS-silica (40–60%) hybrid porous scaffolds were found in the range of 150–250 kPa due to the high porosity along the freezing direction [37]. Increasing silica content caused elastic-brittle deformation behaviour [40].

3.1.7. Protein adsorption

Protein adsorption capacity of a biomaterial is one of the main factors that affect its biocompatibility. The cell-material interaction on surface is considered as the major factor for cell attachment and serum proteins play important role in cell adhesion [41]. This interaction provided by protein adsorption on material surface, is induced by body fluid absorption of biomaterial at the defect site. After this absorption process, cells-adsorbed protein layer interaction initiates on material surface [42]. Protein adsorption on CS surface was measured as 108 μg/ml. Highest protein adsorption was determined in CS-5%POSS scaffolds with 223 μg/ml (Fig. 4). The increase in protein adsorption arises from the enhanced surface area due to POSS nanoparticle incorporation. Similarly, literature studies show that silica incorporation enhances the protein adsorption on the scaffold surface [43,44].

3.1.8. Enzymatic degradation

Lysozyme is mostly used for degradation studies of CS and depolymerizes N-acetylated CS in human serum by breaking its glycosidic bonds via hydrolysis [29]. This degradation process is related with the acetylation degree of CS where high acetylation induces faster degradation [45]. Since it is hydrophilic polymer, water diffusion into CS is faster than degradation causing bulk erosion. CS is degraded in two stages: it interacts with water and swells in first stage which initiates the cleavage of chemical bonds and causes degradation. In second stage, CS is degraded and weight loss is observed [46]. Similarly, CS-POSS scaffolds absorbed enzymatic solution and swelled at first period of incubation (1–7 days), then showed an increase in weight loss % trend at 7–28 days (Fig. 5c). High degree of acetylation of CS (75–85%) induced a drastic increase in weight loss % for 21 days. This arises from cleavage of CS bonds with lysozyme on scaffold surface [47]. Consequently, scaffolds showed comparatively faster degradation rate in the first weeks. Similarly, the biodegradation of CS films showed that the degradation rate generally appeared to slow down after initial weight loss. It is concluded that degradation rate decrease was observed due to the loss of appropriate hexasaccharide sequences and the lack of consecutive N-acetylglucosamine residues with very low degree of acetylation (DA) during the process [29]. In addition, POSS nanoparticles increased the degradation rate of CS scaffolds due to the possible dissolution from the surface as mentioned in literature [44,48]. CS-20%POSS groups distinctly showed the highest weight loss at 21th day of incubation. This increase in weight loss may arise from its dissimilarity in 3D structure which was observed in micro-CT analysis.

3.1.9. Water uptake capacity

Swelling property has a significant function at the defect site during the interaction with body fluids. Biomaterial should possess hydrophilic structure to perform efficent absorption of body fluid and blood to interact with the body fluid contents (i.e. proteins, minerals). Thus, this process leads to protein adsorption on material surface which induces the interaction of biomaterial with surrounding cells. Therefore, water uptake capacity and protein adsorption properties are highly interrelated factors in biomaterial design. In this study, scaffolds were incubated in 1× PBS solution at 37 °C to simulate body fluid conditions. The swelling ratio of CS matrix increased in the range of 29.1–32 due to POSS incorporation (Fig. 5a). Similarly, in literature, silica loading in polymer matrix enhanced the water uptake capacity positively due to its hydrophilic structure [9,49].

3.1.10. Mineralization on material surface

Biomineralization is the major process for bone regeneration that controls the release of ions for Ca/P nucleation and mineral growth as apatite deposition [50]. Mineralization studies on CS-POSS nanocomposites were performed with different m-SBF solutions (1× and 10×). SEM images, EDX and XRD data of scaffolds immersed in 1× and 10× SBF solution were given in supplementary file (Supplementary Figs. S1 and S2). Ideal stochiometric ratio of Ca:P in hydroxyapatite structure is 1.67. However, bone actually exhibits a Ca:P ratio ranging from 1.3:1 to 1.9:1. This deviation mainly arises from the carbonated groups, substitution of other cations, and protonation of phosphate groups in the crystal lattice [51]. SEM images of CS scaffolds immersed in 1× m-SBF showed that globular apatite formation was obtained with heterogeneous distribution on surface. However, POSS incorporated scaffolds immersend in 1× SBF solution induced both globular and needle-like apatite crystals and these structures coated CS-POSS surface after 7–21 days of incubation. EDX analysis of 5–10%POSS incorporated scaffolds which were incubated in 1× m-SBF solution showed similarity with stochiometric Ca/P (1.67) of bone mineral at 7th day. However, at higher POSS concentrations (20–40%), significantly higher Ca deposition was observed on nanocomposite surfaces due to the possible calcium silicate formation. Silica networks degrade, and this causes silanol (Si—OH) formation on material surface which takes part in apatite formation through hydration and dissolution. These Si—OH groups posssess proper sites for Ca/P nucleation which chelate the calcium ions (Ca^{2+}). Calcium silicate formations consecutively gain more positive charges and interact with phosphate ions. Then, amorphous calcium phosphate (ACP) is formed by this interaction. Clusters which reached critical size, trigger apatite nucleation, finally nano-crystalline apatite layer is formed [43,44]. Similarly, literature studies indicated that the mineralization initiated with silanol groups which have specific surface sites, serving a function in Ca/P nucleation [48,52–54]. The effect of POSS nanoparticles and bioactive glass particles were compared on the bioactivity of dental adhesive by observing Ca/P precipitation. It was indicated that POSS nanoparticles rendered the bioactivity [25]. Mineralization study was also performed in 10× m-SBF solution for 14 days of incubation. SEM images of CS-POSS scaffold surfaces at 7 and 14th days of incubation were observed with SEM and given in supplementary file (Supplementary Fig. S2). SEM images with higher magnification showed that, apatite formation was not observed on CS scaffolds at 7th day. However, globular apatite formation was observed on CS-POSS scaffold surface as coated layer at 14 days of immersion in 10× m-SBF (Fig. 6). This calcium-phosphate formation as globular apatite layer transforms into thermodynamically stable crystalline form by dissolution and recrystallization process. At 14th day of immersion, apatite globules were located on CS-POSS scaffolds surface homogenously and apatite layer was observed on 40% POSS incorporated scaffolds. XRD patterns of mineralized scaffolds immersed in 10× m-SBF were depicted in Fig. 6. The characteristic peaks of this CaP formation indexed as (0 0 2), (2 1 1) and (2 2 2) were observed on scaffold surfaces [55]. XRD patterns 10× SBF immersion showed crystalline structure of globular CaP layer on CS-POSS scaffold surface. Characteristic peaks were obtained as (0 0 2), (1 0 2), (2 1 1), (3 1 0), (1 1 3) and (2 2 2) planes of hydroxyapatite. Consequently, POSS nanoparticles provided calcium silicate formation which induced apatite formation on scaffold surface.

3.2. In vitro studies

3.2.1. Cell attachment and spreading

Cell attachment and spreading on material surface are critical factors for cell proliferation and differentiation processes. Enhanced cell attachment and spreading can trigger alterations on intracellular tension and promote the osteogenesis through upregulating the expression of runt-related transcription factor 2 (RUNX2), bone morphogenetic protein 2 (BMP2) and osteocalcin
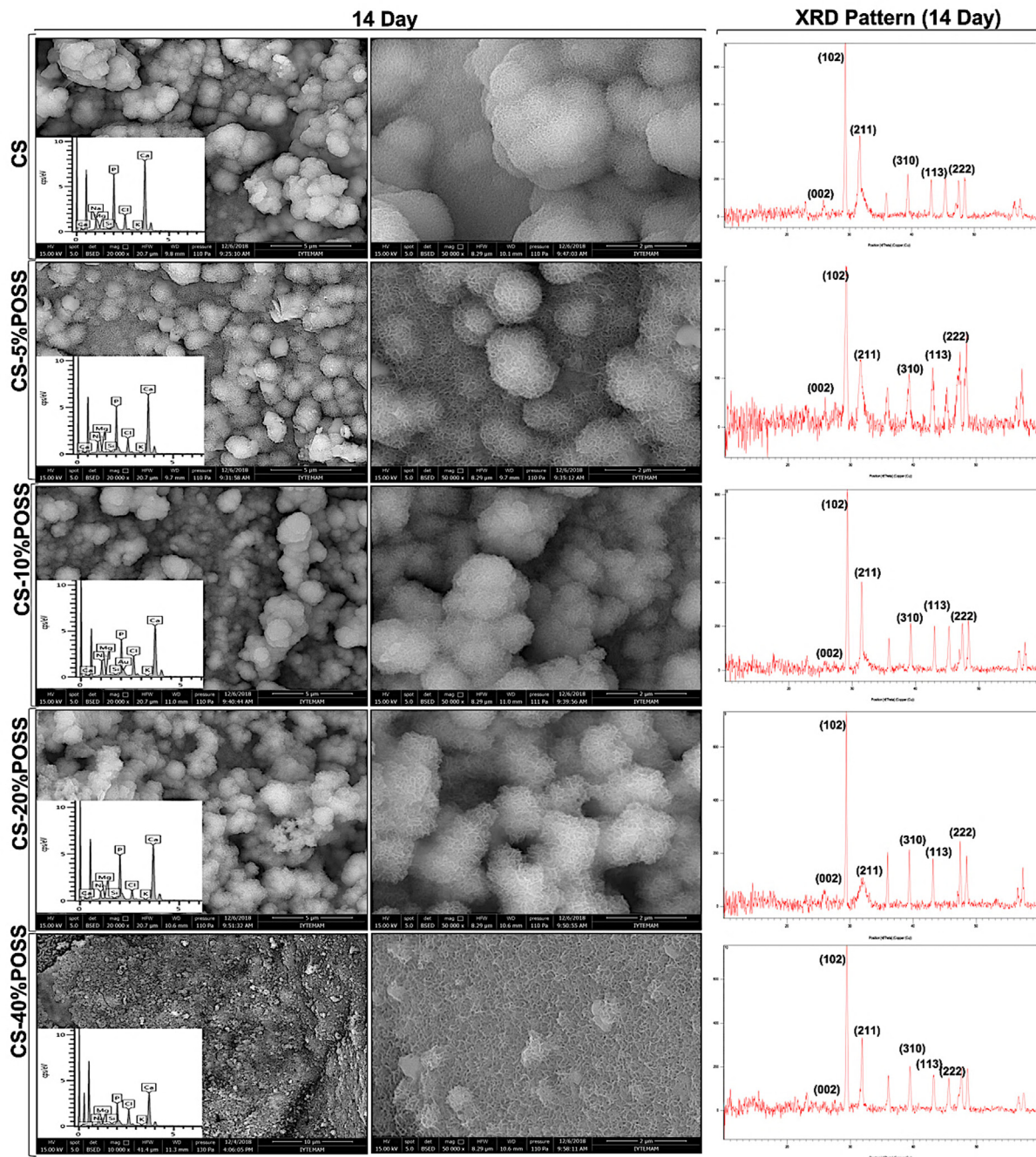
Fig. 6. Scanning electron micrographs, EDX and XRD patterns of apatite formation on CS, CS-POSS nanocomposites immersed in $10\times$ m-SBF at 14th day respectively.

(OCN) as osteogenic markers [56,57]. Generally, osteoblast attachment to biomaterial surface depends on the material properties regarding its surface chemistry, topography and energy which affects the adsorption of biological molecules on material surface. Especially topography has a signifcant effect on cell-surface interaction by improving cell attachment and spreading [58,59]. DAPI-brightfield images showed that POSS incorporation enhanced MG-63 cell attachment and uniform cell spreading compared to CS scaffold (Fig. 7a, e, and g). Fluorescence microscopy images (DAPI-Alexa fluor 555) indicated that MG-63 cells were attached and spread on scaffold surface successfully, subsequently they formed clusters with cell to cell interaction. This positive effect arises from POSS incorporation which alters the surface topography and increases surface roughness. High magnification images demonstrated that MG-63 cells were colonized in close contact with each other and adhered to the pore wall surface with elongations of actin filaments (Fig. 7c, f, and i). SEM images also confirmed that MG-63 cells showed high affinity to POSS incorporated chitosan surface by showing good attachment, spreading and forming clusters on pore walls of scaffold surface (Fig. 7).

3.2.2. In vitro cytotoxicity

In this study, 3T3 cell line was used to determine the cytocompatibility of nanocomposites with respect to ISO 10993 standards. MG-63 and Saos-2 cells were also investigated as model cell lines for cytotoxicity experiments. Results stated that CS-POSS nanocomposites were found cytocompatible with NIH 3T3 cell line.
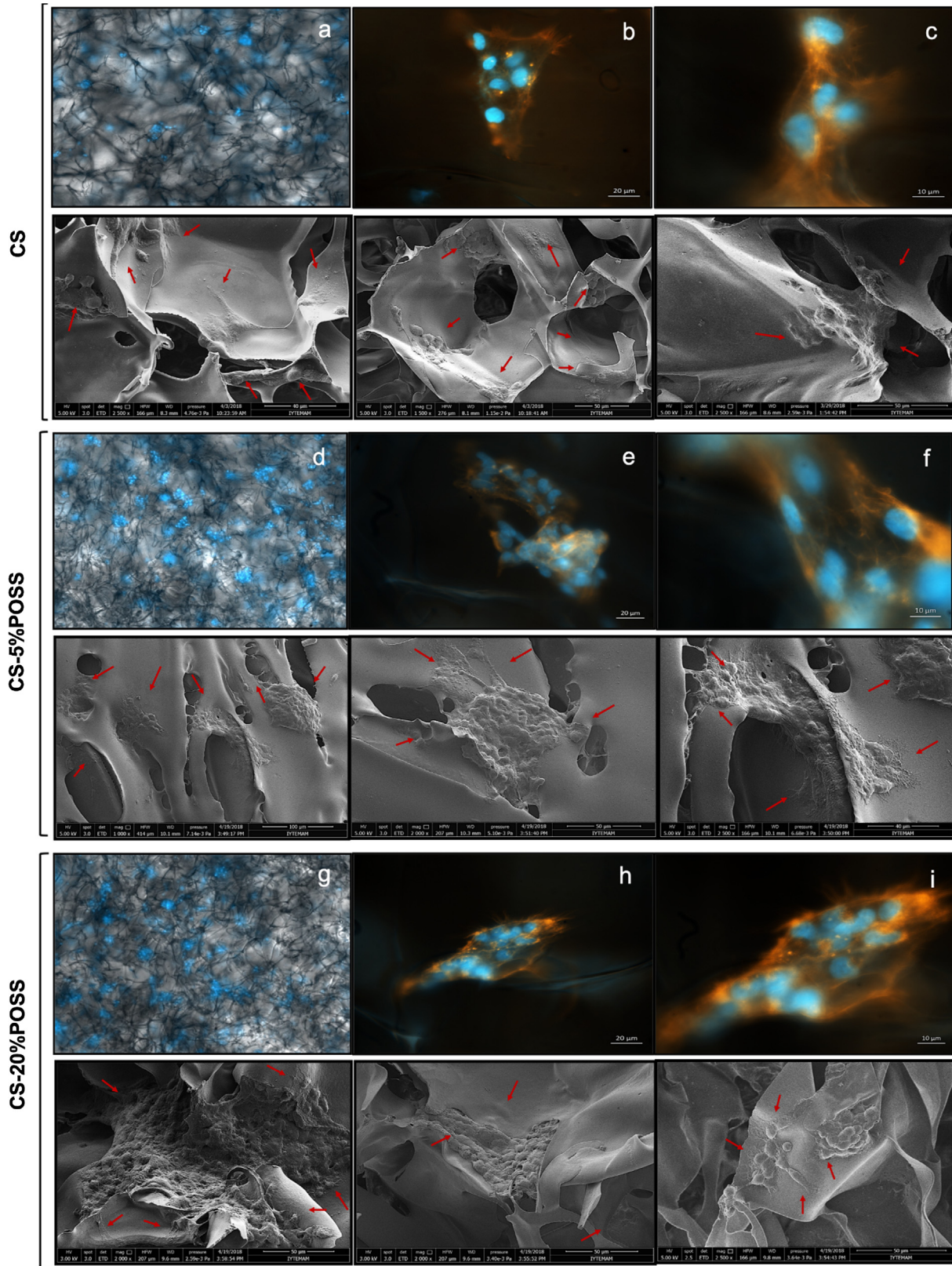
Fig. 7. Fluorescence images of MG-63 cells of cultivated on CS (a, b, c) CS-5% POSS (d, e, f) CS-20% POSS (g, h, and i) nanocomposites at 3rd day (5×, 20× and 40× magnifications); SEM images of MG-63 cells on CS and CS-5% POSS and CS-20% POSS scaffolds at 7th day.

In addition, 5–40% POSS incorporation showed a significant proliferative effect on cells in 24 h. This proliferation led to slight viability decrease further, caused by the contact inhibition for 48 h and 72 h periods. Statistically significant differences were observed between 3%, 10% and 20% POSS in 48 h (Fig. 8a–c). Similarly, literature studies reported nontoxic behaviour for various polymer-
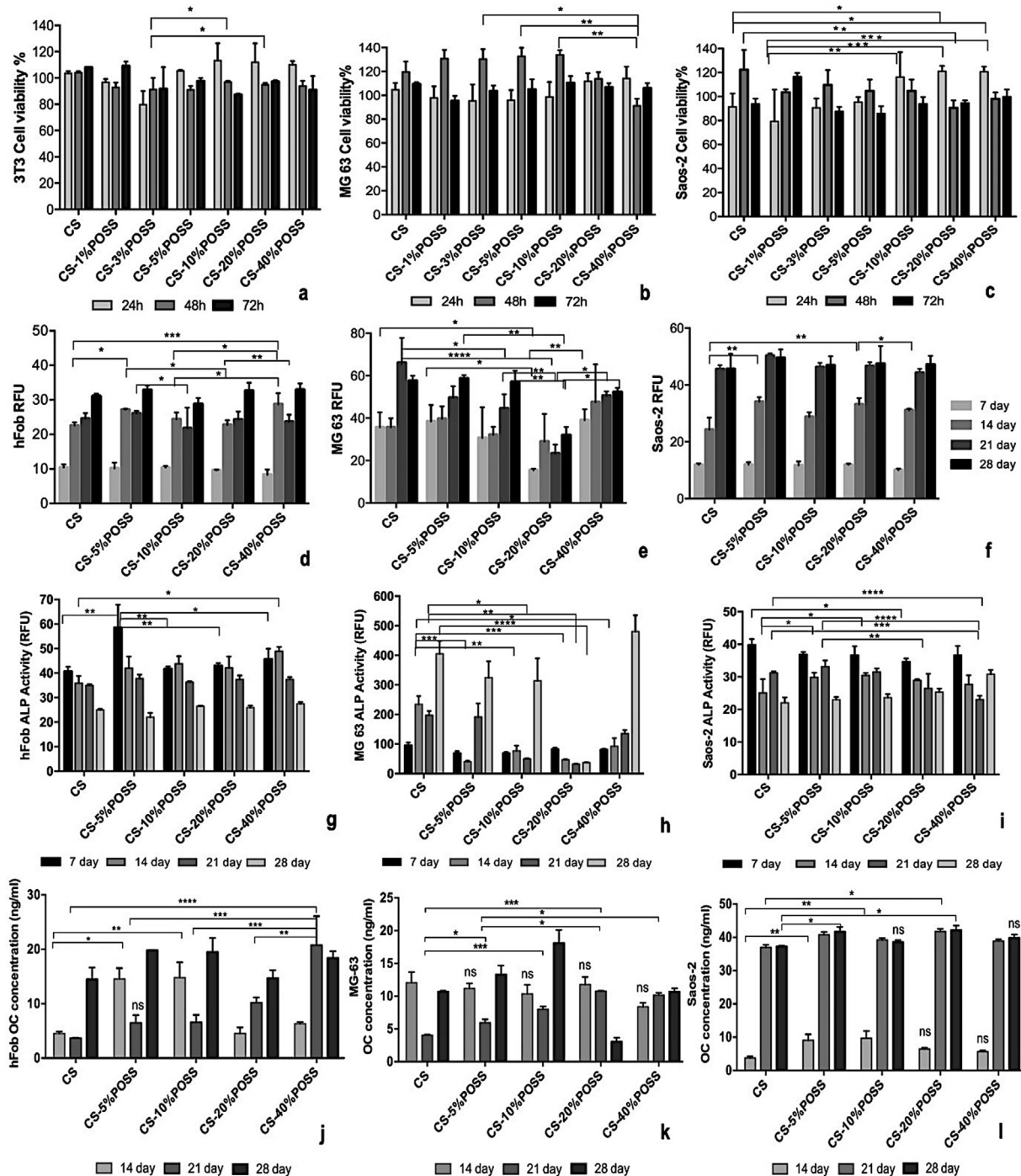
Fig. 8. Cell viability % of 3T3 (a), MG-63 (b), Saos-2 (c) cells incubated with CS-POSS nanocomposite extracts for 24, 48 and 72 h; Proliferation of hFob (d), MG-63 (e), Saos-2 (f) cells on CS-POSS nanocomposites for 28 days. ALP secretion of hFob (g), MG-63 (h), Saos-2 (i) cells at 28 day. Osteocalcin secretion of hFob (j), MG-63 (k), Saos-2 (l) cells on CS-POSS scaffolds at 14, 21 and 28 days. (* represents significant differences).

nSiO$_2$ nanocomposites and indicated that nSiO$_2$ toxicity could be significantly reduced by blending with polymers to form nanocomposites [60].

3.2.3. Cell proliferation and ALP activity

Although osteoblast-like cell lines are known as cell models for bone regeneration, they show different osteoblastic responses concerning several properties such as proliferation kinetics and the osteoid production. However, hFob cells mimic the human osteoblasts by exhibiting similar morphology and osteogenic properties

[61]. MG-63 cells are known as appropriate model cells for studies with regard to the regulation and osteocalcin secretion. However, they are not identified as representative model cells with respect to proliferation and alkaline phosphatase activity [62]. Therefore, CS-POSS scaffolds were investigated with three different cell lines (hFob, MG 63 and Saos-2) having different osteoblastic properties. hFob cells showed a similar proliferation trend for all groups (Fig. 8d). Contrary to literature, MG-63 cells showed a good proliferation an upward trend on CS-POSS (5–10%) scaffolds compared to CS group (Fig. 8e). Saos-2 cells also exhibited an ascending pro-
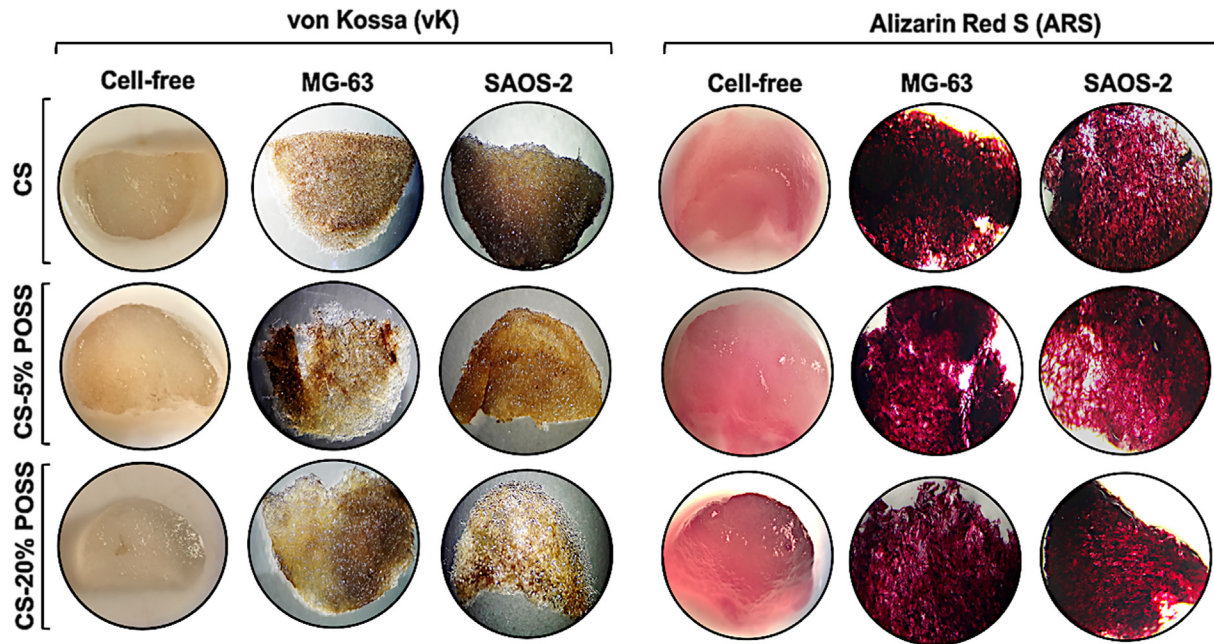
Fig. 9. Stereoimages of vK and ARS stained scaffolds CS, CS-5%POSS and CS-20%POSS scaffolds at 28th day (2× magnification).
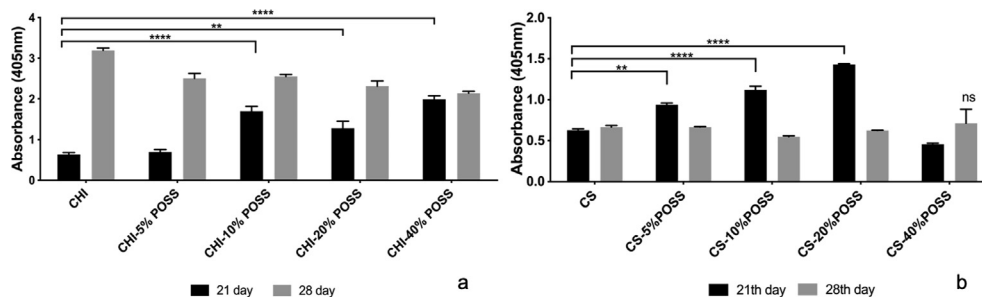

Fig. 10. Detection of calcium deposition with semi-quantitative ARS extraction method for 21 and 28th day MG-63 cells (a) and Saos-2 cells (b) (* represents significant differences).

liferation trend with increasing POSS content (Fig. 8f). POSS agglomerations inducing heterogenity on scaffold structure and increasing organic R groups (metyl ammonium) of POSS may lead to low cell proliferation on scaffolds with higher POSS concentrations. Flourescence microscopy and SEM images also supported results of proliferation studies. MG-63 cells cultivated on CS-POSS nanocomposites formed clusters and showed osteoblastic morphology. Similarly, Keller and co-wokers investigated the effect of silica nanoparticle incorporation in 3D chitosan-scaffolds and concluded that silica nanoparticles promoted osteoblastic spheroid formation and cell proliferation [63].

ALP activity is known as a significant osteogenic differentiation marker at the early stages of bone tissue regeneration. It is reported that, MG-63 cells show low ALP activity and do not mineralise despite being identified as having similar integrin subunit profile to hFob cells [64,65]. However, Saos-2 cells possess higher ALP activity and matrix mineralisation capacity with a more mature osteoblast phenotype [66]. It is also indicated that Saos-2 cells exhibited similar ALP levels at the early stage and growth factor expression to human primary osteoblast cells [65,67–69]. Saos-2 cells on CS-POSS scaffolds showed higher ALP activity at the early incubation periods as expected (7–14 day). (Fig. 8i). At 14th day, 5–10% POSS incorporation significantly increased ALP production of Saos-2 cells. The ALP activity of hFob cells incubated on CS-5% POSS scaffolds exhibited significantly higher ALP production at 7th day

(Fig. 8g). However, all POSS incorporated groups showed higher ALP activity compared to CS group for 7th and 14th day. MG-63 cells secreted ALP at higher levels at the end of cultivation period (Fig. 8h). Nevertheless, ALP activity of MG-63 cells on CS-POSS scaffolds exhibited different increasing trend with incubation time in contrast with Saos-2 and hFob cells. Similar effect of $nSiO_2$ particles on osteogenic activity was reported by incorporation to chitosan/gelatin matrix [43]. In conclusion, hFob and Saos-2 cell lines exhibited similar responses with respect to ALP production as stated in literature. Contrary to the literature studies, MG-63 cells secreted higher amounts of ALP at the late term of cultivation.

3.2.4. Osteocalcin (OC) secretion

OC is secreted at late terms of differentiation and known as a significant osteogenic marker for biomineralization Saos-2 cells secreted higher osteocalcin concentrations for both 21 and 28 days of incubation compared to MG-63 and hFob cell lines. hFob and Saos-2 cells cultivated on 5–10%POSS incorporated scaffolds secreted higher OC compared to chitosan scaffolds at 14th day. In addition, hFob and MG-63 cells produced higher OC on 5–10% POSS groups at 21th day of incubation (Fig. 8j, k and l). Consequently, POSS incorporation promoted OC secretion of cells. Thus, POSS nanoparticles showed positive effect on biomineralization process by inducing OC secretion. This promoting effect may arise from the surface roughness and nanotopographic alterations

obtained with POSS nanoparticle incorporation. Surface alterations can affect cell-material interactions due to cytoskeleton rearrangement and focal adhesion contacts (FACs) formation. Similarly, Filipowska and co-workers investigated the effet of silica particles in chitosan/collagen based hydrogels and indicated that silica particles promoted the osteogenic differentiation of hBMSCs by inducing OC expression [70].

3.2.5. Biomineralization

Surface and cross section of scaffolds are observed to detect mineral formation at the outer and inner parts (Fig. 9). Cell-free scaffold groups were stained and observed under stereomicroscope to compare with cell incubated groups and indicate the color change resulting from biomineralization. Stereoimages showed that cell-free groups slightly absorbed silver nitrate and ARS dye. However, no significant color change was observed. Phosphate deposition was homogeneously distributed on CS scaffolds. Stereoimages showed that POSS incorporation induced mineral formation of cells. Phosphate deposition was heterogenously accumulated at central and peripheral regions of CS-20%POSS group due to non-homogenous cell distribution. This anisotropic distribution may arise from morphological variations regarding to the pore size differences in structure as indicated in micro CT images. Stereoimages indicated that CS-POSS nanocomposites induced calcium deposition of MG-63 and Saos-2 cells. However, distinctive colour difference couldn't be observed due to the possible dye absorbtion of chitosan matrix. Thus, ARS extracts were analysed semi-quantitatively to distinguish the calcium mineral deposition difference with POSS incorporation and indicate the difference between groups. Results showed that, POSS incorporation enhanced calcium deposition on MG-63 cell cultured scaffolds for 28 days. This increase may arise from the pre-osteoblastic nature of MG- 63 cells. This pre-osteoblastic characteristic leads to high proliferation potential causing cell density effect on osteoblastic markers. Thus, MG-63 cells are found inconsistent for mature osteoblastic biomineralization [64,65,69]. However, Saos-2 cells show mature osteoblast phenotype and induce biomineralization by expressing osteoblastic markers such as osteocalcin (OC), bone sialoprotein (BSP) and type I collagen [61,66]. Saos-2 cells induced calcium deposition at 21th day of incubation with increasing POSS concentration up to 20%POSS (Fig. 10). The Ca deposition of Saos-2 cells decreased on CS-40%POSS compared to other groups. This may arise from the possible agglomerations of POSS nanoparticles in chitosan matrix. This may affect the mechanical strength and cell-material interaction in biomineralization process. The decrease in mechanical strength is discussed previously in Fig. 5, Section 3.1.6.

4. Conclusion

This study showed that, POSS nanoparticles have promising effects as a bioactive reinforcement for bone regeneration. POSS incorporation induced favorable effects on cell attachment by altering topography and enhancing surface roughness which are important factors for osteoblast differentiation. CS-POSS scaffolds showed highly porous (82–90%) uniform structures and supplied suitable environment for cell proliferation. Besides, POSS incorporation enhanced the mechanical properties, water uptake capacity of CS scaffolds as well as inducing the mineral deposition and apatite formation on surface. POSS nanoparticles were found to be cytocompatible with fibroblast and osteoblast-like cells. CS-POSS scaffolds enhanced important osteogenic markers for bone regeneration as ALP activity, osteocalcin secretion and mineral formation. Consequently, POSS nanoparticles could be considered as a promising bioactive agent for bone tissue engineering. Further-

more, different POSS structures could be used as reinforcements and the effect of this structural differences can be examined to design novel nanocomposites.

Acknowledgments

Appendix A. Supplementary material

Mineralization study and porosity results were given in supplementary file in detail (Fig. S1, Fig. S2 and Table S1). Supplementary data to this article can be found online at https://doi.org/10.1016/j.ijbiomac.2019.10.006.

References

[1] H.Ç. Arca, S. Şenel, Chitosan based systems for tissue engineering Part 1: hard tissues, J. Pharm. Sci. 33 (2008) 35–49.

[2] I. Kim, S. Seo, H. Moon, M. Yoo, I. Park, B. Kim, C. Cho, Chitosan and its derivatives for tissue engineering applications, Biotechnol. Adv. 26 (2008) 1–21, https://doi.org/10.1016/j.biotechadv.2007.07.009.

[3] A. Di Martino, M. Sittinger, M.V. Risbud, Chitosan: a versatile biopolymer for orthopaedic tissue-engineering, Biomaterials 26 (2005) 5983–5990, https://doi.org/10.1016/j.biomaterials.2005.03.016.

[4] S.L. Chew, K. Wang, S.P. Chai, K.L. Goh, Elasticity, thermal stability and bioactivity of polyhedral oligomeric silsesquioxanes reinforced chitosan-based microfibres, J. Mater. Sci. Mater. Med. 22 (2011) 1365–1374, https://doi.org/10.1007/s10856-011-4318-3.

[5] K.B. Narayanan, N. Sakthivel, Green synthesis of biogenic metal nanoparticles by terrestrial and aquatic phototrophic and heterotrophic eukaryotes and biocompatible agents, Adv. Colloid Interf. Sci. 169 (2011) 59–79, https://doi.org/10.1016/j.cis.2011.08.004.

[6] A. Salama, R.E. Abou-Zeid, M. El-Sakhawy, A. El-Gendy, Carboxymethyl cellulose/silica hybrids as templates for calcium phosphate biomimetic mineralization, Int. J. Biol. Macromol. 74 (2015) 155–161, https://doi.org/10.1016/j.ijbiomac.2014.11.041.

[7] M. Arora, E. Arora, The Promise of Silicon: bone regeneration and increased bone density, J. Arthrosc. Jt. Surg. 4 (2017) 103–105, https://doi.org/10.1016/j.jajs.2017.10.003.

[8] G.R. Beck, S.W. Ha, C.E. Camalier, M. Yamaguchi, Y. Li, J.K. Lee, M.N. Weitzmann, Bioactive silica-based nanoparticles stimulate bone-forming osteoblasts, suppress bone-resorbing osteoclasts, and enhance bone mineral density in vivo, Nanomed. Nanotechnol. Biol. Med. 8 (2012) 793–803, https://doi.org/10.1016/j.nano.2011.11.003.

[9] K. Madhumathi, P.T. Sudheesh Kumar, K.C. Kavya, T. Furuike, H. Tamura, S.V. Nair, R. Jayakumar, Novel chitin/nanosilica composite scaffolds for bone tissue engineering applications, Int. J. Biol. Macromol. 45 (2009) 289–292, https://doi.org/10.1016/j.ijbiomac.2009.06.009.

[10] V. Puchol, J. El Haskouri, J. Latorre, C. Guillem, A. Beltrán, D. Beltrán, P. Amorós, Biomimetic chitosan-mediated synthesis in heterogeneous phase of bulk and mesoporous silica nanoparticles, Chem. Commun. (2009) 2694–2696, https://doi.org/10.1039/b821308a.

[11] C.J. Wu, A.K. Gaharwar, P.J. Schexnailder, G. Schmidt, Development of biomedical polymer-silicate nanocomposites: a materials science perspective, Materials (Basel) 3 (2010) 2986–3005, https://doi.org/10.3390/ma3052986.

[12] D.M. Reffitt, N. Ogston, R. Jugdaohsingh, H.F.J. Cheung, B.A.J. Evans, R.P.H. Thompson, J.J. Powell, G.N. Hampson, Orthosilicic acid stimulates collagen type 1 synthesis and osteoblastic differentiation in human osteoblast-like cells in vitro, Bone 32 (2003) 127–135, https://doi.org/10.1016/S8756-3282(02)00950-X.

[13] M. Dong, G. Jiao, H. Liu, W. Wu, S. Li, Q. Wang, D. Xu, X. Li, H. Liu, Y. Chen, Biological silicon stimulates collagen type 1 and osteocalcin synthesis in human osteoblast-like cells through the BMP-2/Smad/RUNX2 signaling

pathway, Biol. Trace Elem. Res. 173 (2016) 306–315, https://doi.org/10.1007/s12011-016-0686-3.

[14] Ł. John, Selected developments and medical applications of organic–inorganic hybrid biomaterials based on functionalized spherosilicates, Mater. Sci. Eng. C 88 (2018) 172–181, https://doi.org/10.1016/j.msec.2018.02.007.

[15] S.W. Ha, M. Viggeswarapu, M.M. Habib, G.R. Beck, Bioactive effects of silica nanoparticles on bone cells are size, surface, and composition dependent, Acta Biomater. 82 (2018) 184–196, https://doi.org/10.1016/j.actbio.2018.10.018.

[16] J. Wu, P.T. Mather, POSS polymers: physical properties and biomaterials applications, Polym. Rev. 49 (2009) 25–63, https://doi.org/10.1080/15583720802656237.

[17] J. Cho, M.S. Joshi, C.T. Sun, Effect of inclusion size on mechanical properties of polymeric composites with micro and nano particles, Compos. Sci. Technol. 66 (2006) 1941–1952, https://doi.org/10.1016/j.compscitech.2005.12.028.

[18] H. Ghanbari, B.G. Cousins, A.M. Seifalian, A nanocage for nanomedicine: polyhedral oligomeric silsesquioxane (POSS), Macromol. Rapid Commun. 32 (2011) 1032–1046, https://doi.org/10.1002/marc.201100126.

[19] D. Xu, L.S. Loo, K. Wang, Characterization and diffusion behavior of chitosan–POSS composite membranes, J. Appl. Polym. Sci. 122 (2011) 427–435, https://doi.org/10.1002/app.34146.

[20] L. Cai, J. Chen, A.J. Rondinone, S. Wang, Injectable and biodegradable nanohybrid polymers with simultaneously enhanced stiffness and toughness for bone repair, Adv. Funct. Mater. 22 (2012) 3181–3190, https://doi.org/10.1002/adfm.201200457.

[21] F. Renò, F. Carniato, L. Rizzi, L. Marchese, M. Laus, D. Antonioli, POSS/gelatin-polyglutamic acid hydrogel composites: preparation, biological and mechanical characterization, J. Appl. Polym. Sci. 129 (2013) 699–706, https://doi.org/10.1002/app.38789.

[22] R.Y. Kannan, H.J. Salacinski, P.E. Butler, A.M. Seifalian, Polyhedral oligomeric silsesquioxane nanocomposites: the next generation material for biomedical applications, Acc. Chem. Res. 38 (2005) 879–884, https://doi.org/10.1021/ar050055b.

[23] P. Majumdar, J. He, E. Lee, A. Kallam, N. Gubbins, S.J. Stafslien, J. Daniels, B.J. Chisholm, Antimicrobial activity of polysiloxane coatings containing quaternary ammonium-functionalized polyhedral oligomeric silsesquioxane, J. Coatings Technol. Res. 7 (2010) 455–467, https://doi.org/10.1007/s11998-009-9197-x.

[24] M.D. Fernández, M.J. Fernández, M. Cobos, Effect of polyhedral oligomeric silsesquioxane (POSS) derivative on the morphology, thermal, mechanical and surface properties of poly(lactic acid)-based nanocomposites, J. Mater. Sci. 51 (2016) 3628–3642, https://doi.org/10.1007/s10853-015-9686-5.

[25] M. Rizk, L. Hohlfeld, L.T. Thanh, R. Biehl, N. Lühmann, D. Mohn, A. Wiegand, Bioactivity and properties of a dental adhesive functionalized with polyhedral oligomeric silsesquioxanes (POSS) and bioactive glass, Dent. Mater. 33 (2017) 1056–1065, https://doi.org/10.1016/j.dental.2017.06.012.

[26] Y.M. Ha, T. Amna, M.H. Kim, H.C. Kim, S.S.M. Hassan, M.S. Khil, Novel silicificated PVAc/POSS composite nanofibrous mat via facile electrospinning technique: potential scaffold for hard tissue engineering, Colloids Surf. B Biointerf. 102 (2013) 795–802, https://doi.org/10.1016/j.colsurfb.2012.09.018.

[27] C. Gomez-Sanchez, T. Kowalczyk, G. Ruiz De Eguino, A. Lopez-Arraiza, A. Infante, C.I. Rodriguez, T.A. Kowalewski, M. Sarrionandia, J. Aurrekoetxea, Electrospinning of poly(lactic acid)/polyhedral oligomeric silsesquioxane nanocomposites and their potential in chondrogenic tissue regeneration, J. Biomater. Sci. Polym. Ed. 25 (2014) 802–825, https://doi.org/10.1080/09205063.2014.910151.

[28] S. Tamburaci, F. Tihminlioglu, Novel poss reinforced chitosan composite membranes for guided bone tissue regeneration, J. Mater. Sci. Mater. Med. 29 (2018) 1–14, https://doi.org/10.1007/s10856-017-6005-5.

[29] T. Freier, H.S. Koh, K. Kazazian, M.S. Shoichet, Controlling cell adhesion and degradation of chitosan films by N-acetylation, Biomaterials 26 (2005) 5872–5878, https://doi.org/10.1016/j.biomaterials.2005.02.033.

[30] A. Oyane, H.M. Kim, T. Furuya, T. Kokubo, T. Miyazaki, T. Nakamura, Preparation and assessment of revised simulated body fluids, J. Biomed. Mater. Res. - Part A 65 (2003) 188–195, https://doi.org/10.1002/jbm.a.10482.

[31] A.C. Tas, S.B. Bhaduri, Rapid coating of Ti6Al4V at room temperature with a calcium phosphate solution similar to 10× simulated body fluid, J. Mater. Res. 19 (2004) 2742–2749.

[32] S. Tamburaci, F. Tihminlioglu, Biosilica incorporated 3D porous scaffolds for bone tissue engineering applications, Mater. Sci. Eng. C 91 (2018) 274–291, https://doi.org/10.1016/j.msec.2018.05.040.

[33] C.D. Hoemann, H. El-Gabalawy, M.D. McKee, In vitro osteogenesis assays: influence of the primary cell source on alkaline phosphatase activity and mineralization, Pathol. Biol. 57 (2009) 318–323, https://doi.org/10.1016/j.patbio.2008.06.004.

[34] S.H. Phillips, T.S. Haddad, S.J. Tomczak, Developments in nanoscience: polyhedral oligomeric silsesquioxane (POSS)-polymers, Curr. Opin. Solid State Mater. Sci. 8 (2004) 21–29, https://doi.org/10.1016/j.cossms.2004.03.002.

[35] C. Pandis, S. Madeira, J. Matos, A. Kyritsis, J.F. Mano, J.L.G. Ribelles, Chitosan-silica hybrid porous membranes, Mater. Sci. Eng. C 42 (2014) 553–561, https://doi.org/10.1016/j.msec.2014.05.073.

[36] F. Baino, S. Fiorilli, C. Vitale-Brovarone, Bioactive glass-based materials with hierarchical porosity for medical applications: review of recent advances, Acta Biomater. 42 (2016) 18–32, https://doi.org/10.1016/j.actbio.2016.06.033.

[37] D. Wang, F. Romer, L. Connell, C. Walter, E. Saiz, S. Yue, P.D. Lee, D.S. McPhail, J. V. Hanna, J.R. Jones, Highly flexible silica/chitosan hybrid scaffolds with

oriented pores for tissue regeneration, J. Mater. Chem. B 3 (2015) 7560–7576, https://doi.org/10.1039/c5tb00767d.

[38] H.T. Lu, T.W. Lu, C.H. Chen, F.L. Mi, Development of genipin-crosslinked and fucoidan-adsorbed nano-hydroxyapatite/hydroxypropyl chitosan composite scaffolds for bone tissue engineering, Int. J. Biol. Macromol. 128 (2019) 973–984, https://doi.org/10.1016/j.ijbiomac.2019.02.010.

[39] A.R. Costa-Pinto, R.L. Reis, N.M. Neves, Scaffolds based bone tissue engineering: the role of chitosan, Tissue Eng. Part B Rev. 17 (2011) 331–347, https://doi.org/10.1089/ten.teb.2010.0704.

[40] D. Wang, W. Liu, Q. Feng, C. Dong, Q. Liu, L. Duan, J. Huang, W. Zhu, Z. Li, J. Xiong, Y. Liang, J. Chen, R. Sun, L. Bian, D. Wang, Effect of inorganic/organic ratio and chemical coupling on the performance of porous silica/chitosan hybrid scaffolds, Mater. Sci. Eng. C 70 (2017) 969–975, https://doi.org/10.1016/j.msec.2016.04.010.

[41] K.L. Menzies, L. Jones, The impact of contact angle on the biocompatibility of biomaterials, Optom. Vis. Sci. 87 (2010) 387–399, https://doi.org/10.1097/OPX.0b013e3181da863e.

[42] R. Latour, Biomaterials, protein-surface interactions, Biomater. Biomed. Eng. 1 (2005) 15, https://doi.org/10.1081/E-EBBE-120041856.

[43] K.C. Kavya, R. Jayakumar, S. Nair, K.P. Chennazhi, Fabrication and characterization of chitosan/gelatin/n SiO2 composite scaffold for bone tissue engineering, Int. J. Biol. Macromol. 59 (2013) 255–263, https://doi.org/10.1016/j.ijbiomac.2013.04.023.

[44] J.A. Sowjanya, J. Singh, T. Mohita, S. Sarvanan, A. Moorthi, N. Srinivasan, N. Selvamurugan, Biocomposite scaffolds containing chitosan/alginate/nano-silica for bone tissue engineering, Colloids Surf. B Biointerf. 109 (2013) 294–300, https://doi.org/10.1016/j.colsurfb.2013.04.006.

[45] T. Kean, M. Thanou, Biodegradation, biodistribution and toxicity of chitosan, Adv. Drug Deliv. Rev. 62 (2010) 3–11, https://doi.org/10.1016/j.addr.2009.09.004.

[46] D. Ren, H. Yi, W. Wang, X. Ma, The enzymatic degradation and swelling properties of chitosan matrices with different degrees of N-acetylation, Carbohydr. Res. 340 (2005) 2403–2410, https://doi.org/10.1016/j.carres.2005.07.022.

[47] Y. Wan, A. Yu, H. Wu, Z. Wang, D. Wen, Porous-conductive chitosan scaffolds for tissue engineering II. In vitro and in vivo degradation, J. Mater. Sci. Mater. Med. 16 (2005) 1017–1028, https://doi.org/10.1007/s10856-005-4756-x.

[48] M. Pourhaghgouy, A. Zamanian, M. Shahrezaee, M. Pourbaghi, Physicochemical properties and bioactivity of freeze-cast chitosan nanocomposite scaffolds reinforced with bioactive glass, Mater. Sci. Eng. C 58 (2016) 180–186, https://doi.org/10.1016/j.msec.2015.07.065.

[49] K. Li, H. Sun, H. Sui, Y. Zhang, H. Liang, X. Wu, Q. Zhao, Composite mesoporous silica nanoparticle/chitosan nanofibers for bone tissue engineering, RSC Adv. 5 (2015) 17541–17549, https://doi.org/10.1039/C4RA15232H.

[50] E. Ruiz-Hitzky, K. Ariga, Y.M. Lvov, in: Bio-inorganic Hybrid Nanomaterials: Strategies, Syntheses, Characterization and Applications, John Wiley & Sons, 2008, https://doi.org/10.1002/9783527621446.

[51] S. Behzadi, G.A. Luther, M.B. Harris, O.C. Farokhzad, M. Mahmoudi, Nanomedicine for safe healing of bone trauma: opportunities and challenges, Biomaterials 146 (2017) 168–182, https://doi.org/10.1016/j.biomaterials.2017.09.005.

[52] M. Tanahashi, T. Yao, T. Kokubo, M. Minoda, T. Miyamoto, T. Nakamura, T. Yamamuro, Apatite coating on organic polymers by a biomimetic process, J. Am. Ceram. Soc. (1994), https://doi.org/10.1111/j.1151-2916.1994.tb04508.x.

[53] N.M. Alves, I.B. Leonor, H.S. Azevedo, R.L. Reis, J.F. Mano, Designing biomaterials based on biomineralization of bone, J. Mater. Chem. 20 (2010) 2911, https://doi.org/10.1039/b910960a.

[54] P. Jongwattanapisan, N. Charoenphandhu, N. Krishnamra, S. Meejoo, W. Pon-on, In vitro study of the SBF and osteoblast-like cells on hydroxyapatite/chitosan – silica nanocomposite, Mater. Sci. Eng. C 31 (2011) 290–299, https://doi.org/10.1016/j.msec.2010.09.009.

[55] A. Szewczyk, M. Prokopowicz, Amino-modified mesoporous silica SBA-15 as bifunctional drug delivery system for cefazolin: release profile and mineralization potential, Mater. Lett. 227 (2018) 136–140, https://doi.org/10.1016/j.matlet.2018.05.059.

[56] J.W. Cassidy, J.N. Roberts, C.A. Smith, M. Robertson, K. White, M.J. Biggs, R.O.C. Oreffo, M.J. Dalby, Osteogenic lineage restriction by osteoprogenitors cultured on nanometric grooved surfaces: the role of focal adhesion maturation, Acta Biomater. 10 (2014) 651–660, https://doi.org/10.1016/j.actbio.2013.11.008.

[57] X. Yang, Y. Li, X. Liu, Q. Huang, R. Zhang, Q. Feng, Incorporation of silica nanoparticles to PLGA electrospun fibers for osteogenic differentiation of human osteoblast-like cells, Regen. Biomater. 5 (2018) 229–238, https://doi.org/10.1093/rb/rby014.

[58] K. Anselme, Osteoblast adhesion on biomaterials, Biomaterials 21 (2000) 667–681.

[59] S.C. Rizzi, D.J. Heath, A.G.A. Coombes, N. Bock, M. Textor, S. Downes, C. Zu, Biodegradable polymer/hydroxyapatite composites: surface analysis and initial attachment of human osteoblasts, J. Biomed. Mater. Res.: Off. J. Soc. Biomater. Jpn. Soc. Biomater. Aust. Soc. Biomater. Kor. Soc. Biomater. 55 (4) (2001) 475–486.

[60] S. Deepthi, J. Venkatesan, S. Kim, J.D. Bumgardner, R. Jayakumar, An overview of chitin or chitosan/nano ceramic composite scaffolds for bone tissue engineering, Int. J. Biol. Macromol. 93 (2016) 1338–1353.

[61] C. Pautke, M. Schieker, T. Tischer, A. Kolk, P. Neth, W. Mutschler, S. Milz, Characterization of osteosarcoma cell lines MG-63, Saos-2 and U-2 OS in comparison to human osteoblasts, Anticancer Res. 24 (2004) 3743–3748.

[62] J. Clover, M. Gowenf, Are MG-63 and HOS TE85 human osteosarcoma cell lines representative models of the osteoblastic phenotype?, Bone 15 (1994) 585–591.

[63] L. Keller, M. Gimeno, S. Eap, G. Mendoza, V. Andreu, Q. Wagner, A. Kyzio, Chitosan-based nanocomposites for the repair of bone defects, Nanomed.: Nanotechnol. Biol. Med. 13 (2017) 2231–2240, https://doi.org/10.1016/j.nano.2017.06.007.

[64] M.D. Pierschbacher, S. Dedhar, E. Ruoslahti, S. Argraves, S. Suzuki, An adhesion variant of the MG-63 osteosarcoma cell line displays an osteoblast-like phenotype, Ciba Found. Symp., 1988.

[65] L. Saldaña, F. Bensiamar, A. Boré, N. Vilaboa, Acta Biomaterialia In search of representative models of human bone-forming cells for cytocompatibility studies, Acta Biomater. 7 (2011) 4210–4221, https://doi.org/10.1016/j.actbio.2011.07.019.

[66] E. Murray, D. Provvedini, D. Curran, B. Catherwood, H. Sussman, S. Manolagas, Characterization of a human osteoblastic osteosarcoma cell line (SAOS-2) with high bone alkaline phosphatase activity, J. Bone Miner. Res. (1987), https://doi.org/10.1002/jbmr.5650020310.

[67] G. Bilbe, E. Roberts, M. Birch, D.B. Evans, PCR phenotyping of cytokines, growth factors and their receptors and bone matrix proteins in human osteoblast-like cell lines, Bone (1996), https://doi.org/10.1016/S8756-3282(96)00254-2.

[68] L.G. Rao, M.K. Sutherland, G.S. Reddy, M.L. Siu-Caldera, M.R. Uskokovic, T.M. Murray, Effects of 1alpha,25-dihydroxy-16ene, 23yne-vitamin D3 on osteoblastic function in human osteosarcoma SaOS-2 cells: differentiation-stage dependence and modulation by 17-beta estradiol, Bone (1996).

[69] E.M. Czekanska, M.J. Stoddart, R.G. Richards, J.S. Hayes, In search of an osteoblast cell model for in vitro research, Eur. Cells Mater. (2012), https://doi.org/10.22203/eCM.v024a01.

[70] J. Filipowska, J. Lewandowska-Łańcucka, A. Gilarska, Ł. Niedźwiedzki, M. Nowakowska, In vitro osteogenic potential of collagen/chitosan-based hydrogels-silica particles hybrids in human bone marrow-derived mesenchymal stromal cell cultures, Int. J. Biol. Macromol. 113 (2018) 692–700, https://doi.org/10.1016/j.ijbiomac.2018.02.161.